J Appl Physiol
89: 2030–2040, 2000.

Size distribution of recruited alveolar volumes in airway reopening

BÉLA SUKI,[1] ADRIANO M. ALENCAR,[1,2] JÓZSEF TOLNAI,[3] TIBOR ASZTALOS,[3] FERENC PETÁK,[1,3] MAMATHA K. SUJEER,[1] KEENA PATEL,[1] JIGNISH PATEL,[1] H. EUGENE STANLEY,[2] AND ZOLTÁN HANTOS[3]
[1]*Department of Biomedical Engineering and* [2]*Center for Polymer Studies, Department of Physics, Boston University, Boston, Massachusetts 02215; and* [3]*Department of Medical Informatics and Engineering and Institute of Surgical Research, University of Szeged, Szeged, Hungary*

Received 27 May 1998; accepted in final form 30 June 2000

Suki, Béla, Adriano M. Alencar, József Tolnai, Tibor Asztalos, Ferenc Peták, Mamatha K. Sujeer, Keena Patel, Jignish Patel, H. Eugene Stanley, and Zoltán Hantos. Size distribution of recruited alveolar volumes in airway reopening. *J Appl Physiol* 89: 2030–2040, 2000.—In 11 isolated dog lung lobes, we studied the size distribution of recruited alveolar volumes that become available for gas exchange during inflation from the collapsed state. Three catheters were wedged into 2-mm-diameter airways at total lung capacity. Small-amplitude pseudorandom pressure oscillations between 1 and 47 Hz were led into the catheters, and the input impedances of the regions subtended by the catheters were continuously recorded using a wave tube technique during inflation from −5 cmH_2O transpulmonary pressure to total lung capacity. The impedance data were fit with a model to obtain regional tissue elastance (Eti) as a function of inflation. First, Eti was high and decreased in discrete jumps as more groups of alveoli were recruited. By assuming that the number of opened alveoli is inversely proportional to Eti, we calculated from the jumps in Eti the distribution of the discrete increments in the number of opened alveoli. This distribution was in good agreement with model simulations in which airways open in cascade or avalanches. Implications for mechanical ventilation may be found in these results.

atelectasis; lung elastance; avalanches; power law; percolation; gas exchange

THE INSPIRED AIR AT LOW LUNG volumes is preferentially distributed to the upper regions of the lung as a result of the presence of airway closure (19). Airways start to close off when lung volume is lowered below the closing volume (CV) (16). In normal lungs, functional residual capacity (FRC) represents a higher lung volume than CV; hence, during normal breathing, end-expiratory lung volume does not reach CV, and closure does not take place. However, in the immature lung (33), with advancing age (16), in obesity (11), in emphysema (10), and possibly in other lung diseases such as asthma (28), closure may occur during normal breathing at end expiration. The transpulmonary pressure (Ptp, defined as airway pressure minus pleural pressure) at which the closed airways reopen during inspiration is always higher than the Ptp at which closure develops (22). Thus closure can easily lead to an inhomogeneous alveolar ventilation and, hence, an impaired gas exchange (4).

With regard to lung function in the presence of airway closure, the most important quantity is the amount of alveolar volume available for gas exchange. This alveolar volume is decreased at end expiration and is recruited during inspiration when airways reopen. Whereas the physical factors determining the actual process of closure and reopening in individual airways have been studied in great detail (8, 13, 23, 24), very few studies have addressed how airways reopen in situ (20, 22, 26, 34). The fact that airways constitute a tree structure may lead to interactions among reopening of airway segments that are otherwise spatially well separated. It is not clear how such a spatial interaction during the reopening process can influence the distribution of recruited alveolar volumes and, hence, gas exchange in the lung.

Recently, Peták et al. (26) and Otis et al. (21, 22) studied airway closure and opening by measuring the terminal airway resistance (R_t) during deflation and inflation and found that, during inflation, R_t decreased in a series of discrete jumps. A statistical interpretation of this process was provided by Suki et al. (32). According to this interpretation, airways open in cascades or avalanches triggered by overcoming a hierarchy of critical opening threshold pressures along the airway tree. More recently, Barabási et al. (3) developed an analytic statistical mechanical model of the first avalanches during an inflation by mapping the inflation problem to a percolation problem in a tree structure. This model has been further developed by Sujeer et al. (30) to include all avalanches during an inflation and to predict the distribution of the sizes of alveolar volumes that open via avalanches. Their simulations predicted that this distribution is wide follow-

Address for reprint requests and other correspondence: B. Suki, Dept. of Biomedical Engineering, Boston University, 44 Cummington St., Boston, MA 02215 (E-mail:bsuki@bu.edu).

The costs of publication of this article were defrayed in part by the payment of page charges. The article must therefore be hereby marked "*advertisement*" in accordance with 18 U.S.C. Section 1734 solely to indicate this fact.

ing a power law and is independent of airway wall and alveolar tissue elasticity.

The purpose of this study is to experimentally test these predictions by indirectly measuring the sizes of terminal air spaces that open during inflation and by comparing their distribution with that predicted by previous model simulations (30). To achieve this goal, we used a technique developed by Hantos et al. (9) that is able to measure the input impedance of small subtrees of the tracheobronchial tree in isolated lungs. We measured these impedances during inflation and then fit the spectra with a model from which we can estimate the regional tissue elastance (Eti) of the subtrees as a function of inflation pressure. We found that, during inflation, Eti decreases in many discrete steps spanning a wide range of sizes. By assuming that Eti is inversely related to the size of the alveolar space that communicates with the trachea, we estimated the distribution of these steplike volume changes in terminal air spaces due to airway opening.

METHODS

Preparation of lobes. We obtained 11 lung lobes from 8 mongrel dogs weighing 18–24 kg. The animals were anesthetized with pentobarbital sodium (30 mg/kg), treated with heparin (5,000 units), and exsanguinated via a femoral artery. The lungs were removed, and selected lobes were cannulated in the main bronchus with an 8- to 12-mm-ID metal tube. First, the lobe was inflated to a positive airway pressure of 30 cmH_2O and checked for leaks. The bronchial cannula was attached to a short tube mounted in the lid of an airtight glass box (15 liters). A schematic drawing of the setup is shown in Fig. 1. The cannula was open to atmosphere so that Ptp, measured in the box with respect to atmosphere with a transducer (model MP-45, Validyne; 50 cmH_2O), could be conveniently adjusted by pumping or sucking air into or out of the box with the use of a dual-membrane pump (model MP 03 Ez, Otto Huber). The lobe was suspended in the closed box and reinflated to 30 cmH_2O Ptp by creating a -30-cmH_2O pressure in the box. A slightly curved 20- to 30-cm-long (L_2) polyethylene catheter (1.53 mm ID, 2 mm OD) with a bell-shaped metal ending was led through the lid into the main bronchus until it wedged in a peripheral airway. After a deflation to 5 cmH_2O Ptp, the catheter was gently pulled back to ensure that the rim of the metal ending was fixed in the bronchial wall. This procedure was repeated with two more catheters that were guided to different peripheral regions. The bottom of the box was covered with wet gauze to keep the lobe surface moist.

Impedance measurements and signal processing. The three wedged catheters were connected to a loudspeaker-in-box system through identical tubes of the same polyethylene material (42 cm long, L_1; Fig. 1). These sections served as wave guides and were equipped with side taps and miniature transducers (model 33NA002D, ICS) to measure the lateral pressures at their distal ends (P_2) and the common entrance pressure in the loudspeaker chamber (P_1). The loudspeaker was driven by a computer-generated pseudorandom signal having a period of 1 s and containing 17 discrete frequency components between 1 and 47 Hz. The spectrum of the signal was flat, and the phase angles were chosen to minimize the peak-to-peak value of the signal. The power amplifier of the loudspeaker was adjusted so that the peak-to-peak value of P_1 was <1 cmH_2O. Forced oscillations were continuously

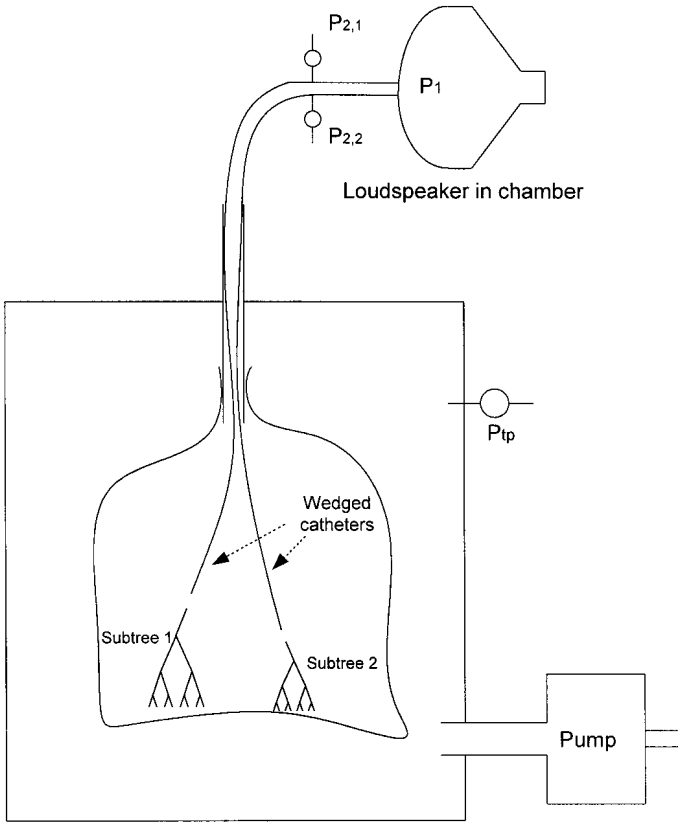

Fig. 1. Schematic of the experimental setup. The lung is inflated in the box by means of a vacuum pump. Polyethylene *catheters 1* and *2* are wedged in peripheral airways. Pressure oscillations are generated by a loudspeaker-in-chamber and led into the periphery of the lung via the catheters. Common pressure (P_1) is measured in the loudspeaker box; pressures $P_{2,1}$ and $P_{2,2}$ are measured at the distal ends of the wave guides connecting the catheters and the loudspeaker chamber. Ptp, transpulmonary pressure.

delivered, and P_1 and P_2 were measured while the lobe was slowly inflated from -5 to 30 cmH_2O Ptp in ~160 s. The signals P_1 and P_2 were low-pass filtered (5th-order Butterworth, 50-Hz corner frequency) and digitized at a sampling rate of 256 Hz. The inflation recordings were split into 160 short recordings, each containing 256 time points. The pressure transfer functions P_1/P_2 were computed using fast Fourier transformation for each recording of 256 points, providing a 1-Hz frequency resolution. From the P_1/P_2 spectra, the input impedance of the subtrees (Z_p) subtended by the catheters was derived as the load impedance seen at the distal end of the wedged catheter, as described in detail previously (9)

$$Z_p = Z_0^2 \frac{\tanh(L_2\Gamma) - ZZ_0}{Z\tanh(L_2\Gamma) - Z_0} \quad (1)$$

where Z is defined as (6, 7)

$$Z = \frac{Z_0 \sinh(L_1\Gamma)}{P_1/P_2 - \cosh(L_1\Gamma)} \quad (2)$$

In *Eqs. 1* and *2*, Z_0 and Γ are the characteristic impedance and the complex propagation wave number, respectively, of the wave guide. Z_0 and Γ are determined by the tube geometry and the physical properties of the resident gas and the tube wall. This process was carried out on all recordings, which resulted in 160 complex impedance spectra per cath-

eter and lobe between 1 and 47 Hz as a function of inflation with a time resolution of 1 s.

The ability of the entire system to determine impedance over a wide range of magnitudes was tested in two different ways. First, small glass bottles of different sizes were measured with elastance values similar to those of the airway subtrees. The length of the catheters and the input amplitude were varied to find their optimal values. Second, the catheter end where P_1 is measured was blocked, and the pressure-to-pressure ratio (P_1/P_2) in the closed tube was determined over the 1- to 47-Hz frequency range. P_1/P_2 can then be predicted using wave propagation theory in rigid tubes, which provides a validation of the technique as described previously (15). Both tests were satisfactory, providing evidence that the resolution (ratio of the smallest to the largest elastance) of the wave tube technique was ≤ 0.001.

Parameter estimation and statistical analysis. The Z_p spectra were evaluated on the basis of several simple models of the airway tree and the alveoli. A simplistic view of two neighboring subtrees in the lung and two collateral airways connecting them is shown in Fig. 2*A*. An equivalent electrical model of this structure is shown in Fig. 2*B*. $R_{c,1}$ and $R_{c,2}$ are the resistances of the collateral airways. The electrical model is a simplified version of the model introduced recently by Hantos et al. (9). The model includes two airway resistances (R_1 and R_2) in series, representing the regular airways between the catheter end and the alveoli. Another resistance (R_c) is placed as a shunt pathway between R_1 and R_2 to account for the resistance of the collateral airways connecting the two subtrees (Fig. 2*A*). Thus R_1 can be interpreted as an equivalent resistance of all the airways between the end of the catheter and the collateral airway, and R_2 models all the airways that are peripheral to the collateral airway. The parenchymal tissues are modeled by an ideal elastic component, Eti, connected in series with R_2. Thus R_c is in parallel with R_2 and Eti, which means that it is connected to ground in the electrical model in Fig. 2*B,* since the collateral airway will shunt part of the input flow to the atmosphere through the neighboring subtree shown in Fig. 2*A*.

The model parameters were estimated by means of a global optimization procedure (5) minimizing the root-mean-square error between measured and model impedances. R_1 and R_2, however, were not fit simultaneously, because the features in the Z_p spectra did not allow simultaneous and unique estimation of R_1 and R_2. For each data set corresponding to a single inflation and a single catheter (160 impedance spectra), first R_1 was fixed to zero (*model A* in Fig. 2*C*) and the parameters including R_2 were determined. Next, R_2 was fixed to zero (*model B* in Fig. 2*D*), and all parameters including R_1 were determined for the same data set. These two models differ in the way they represent the major location of the collateral airway resistance. *Model A* incorporates the notion that the collateral airway is closer to the end of the catheter. Thus $R_{c,2}$ is large (or infinite) and negligible compared with $R_{c,1}$; hence, R_1 is neglected. *Model B* places the collateral airway closer to the alveoli. Thus $R_{c,1}$ is large (or infinite) and negligible compared with $R_{c,2}$; hence, R_2 is neglected. For a given data set corresponding to a single inflation, the final model parameters were selected on the basis of which model produced smaller errors. However, for a given data set corresponding to one inflation and one region, only one of the models, *model A* or *model B*, was used for all 160 Z_p spectra. The corresponding resistance from *model A* or *model B* was simply denoted by R. Time series were then formed from the model parameters as a function of inflation time. The statistical properties of these time series were

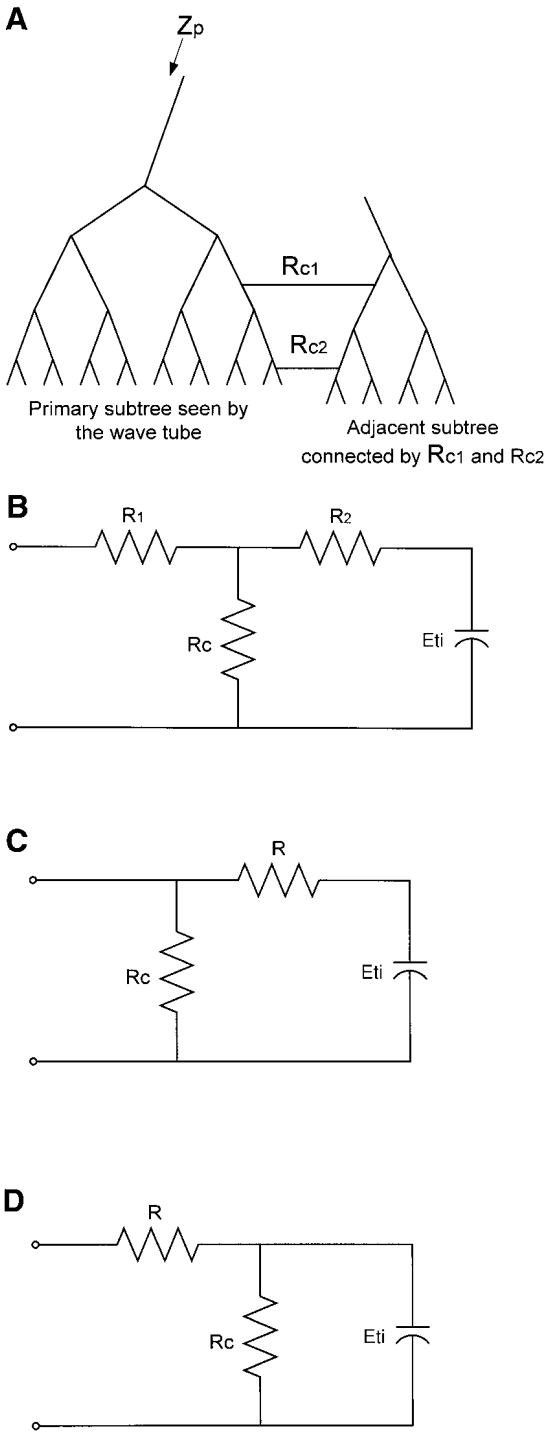

Fig. 2. *A*: schematic representation of a peripheral airway subtree. Z_p, input impedance of the subtree measured by the catheter system (see Fig. 1). An adjacent subtree is also shown connected to the primary subtree via 2 collateral airways ($R_{c,1}$ and $R_{c,2}$). *B*: electrical equivalent analog of the system in *A*. R_1 and R_2, lumped airway resistances of the primary subtree above $R_{c,1}$ and below $R_{c,2}$, respectively; Eti, elastance of the subtree shunted by the lumped collateral airway resistance R_c, which includes $R_{c,1}$ and $R_{c,2}$. *C*: a simplified version of the model in *B* with the notion that the influence of $R_{c,2}$ is small compared with that of $R_{c,1}$; hence, R_1 is neglected. *D*: a simplified version of the model in *B* with the notion that the influence of $R_{c,1}$ is small compared with that of $R_{c,2}$; hence, R_2 is neglected.

evaluated by calculating their probability density distribution function.

Simulation studies. We used the model developed by Sujeer et al. (30) to interpret our measured regional airway resistance and Eti time series. Briefly, the periphery of the airway tree was modeled as a symmetrical binary tree with airway segments that can be closed or opened. At *time 0*, all airways are assumed to be closed. Lung inflation is simulated by applying an external pressure (P_E) at the top of the tree and gradually increasing P_E at a slow rate. Airways are labeled (i,j) with a generation number i ($i = 0, \ldots, M$), where $M = 12$ is the order of the tree ($i = 0$ denotes the root of the tree), and a column number j ($j = 0, \ldots, 2^{i-1}$). A critical opening threshold pressure $P_{i,j}$ is assigned to each airway (i,j), which pops open instantaneously whenever $P_{i,j}$ is smaller than or equal to the pressure in its parent. All pressures are normalized so that, during inflation, P_E increases from 0 to 1, which corresponds to Ptp decreasing from 0 to -30 cmH_2O at total lung capacity (TLC). The values of $P_{i,j}$ were thus between 0 and 1 and were taken from a uniform distribution (3, 30, 32). The alveoli are represented by the last-generation segments in the model. Because of the lack of data in the literature, we assume that these segments behave the same way as the small airways; that is, they are assigned a threshold pressure that is uniformly distributed between 0 and 1.

The inflation process is simulated in the lung model by increasing P_E in small increments. P_E is initially assigned the value $P_{0,0}$, the critical opening threshold pressure of the root or airway (0,0). Since an airway opens when the pressure in its parent equals or exceeds its critical opening threshold pressure, the airway (0,0) now opens, and its pressure is set equal to P_E. Next, the two airways (1,0) and (1,1) are tested to see if they can be opened by this value of P_E (the present pressure in their parent airway), that is, whether $P_E > P_{1,0}$ and/or $P_E > P_{1,1}$. If one or both conditions are met, then the airways (1,0) and/or (1,1) are also opened. This opening is then continued sequentially down the tree until no airway is found with its $P_{i,j} < P_E$. Of particular interest is the fact that a small increase in P_E can lead to an "avalanche" in which many airways open simultaneously (32). When the first avalanche stops, the critical opening threshold pressures of those airways that are still closed but with parents that are now open are examined. P_E is then incremented to the smallest of these threshold pressures, and the pressure in all open airways is updated to this new value. This process is iterated until all airways open. A sequence of avalanches filling a small five-generation tree is demonstrated in Fig. 3.

Airway and alveolar wall tissue elasticity is introduced by requiring that the diameters (and hence the volumes) of the open airways and alveoli depend on P_E. The diameter values are updated with each increase in P_E according to the following exponential pressure-volume relationship taken from the literature (27)

$$v = v_0 + a(1 - e^{bP_E}) \quad (3)$$

where v is lung volume and v_0, a, and b are parameters. Thus a newly opened airway/alveolus will distend, because of the elastic nature of its wall, to a volume that is a function of P_E and so contribute to an avalanche with a volume greater than that of a corresponding airway/alveolus from a rigid tree for the same value of P_E. Gas exchange in the model occurs only in the "opened" alveoli that are in communication with the trachea. Collateral channels were not included in these simulations for the following reason: although collateral channels have a substantial effect on the frequency dependence of regional lung impedance, and hence their inclusion in the model was indispensable, they do not appear to play an important role in the distribution of recruited alveolar volumes. Thus instantaneous lung volume (v) is taken to be proportional to the number of last-generation segments that are connected to the root of the model by the avalanches. Let us denote the elastance of a single alveolus by E_A. When two elastic elements each having an elastic constant of E_A are arranged in parallel, the total elastance is $E_A/2$. Therefore, since the terminal units are in parallel, Eti of the model is taken to be inversely proportional to the number of open terminal units (N) at a given P_E, that is

$$Eti = E_A/N \quad (4)$$

As the avalanches continue to open the tree, Eti will decrease in discrete steps, as demonstrated in Fig. 3. The jumps in Eti, denoted by dE, can be simply related to the changes in the number of open terminal units

$$dE = Eti^1 - Eti^2 = \frac{E_A}{N^1} - \frac{E_A}{N^2} \quad (5)$$

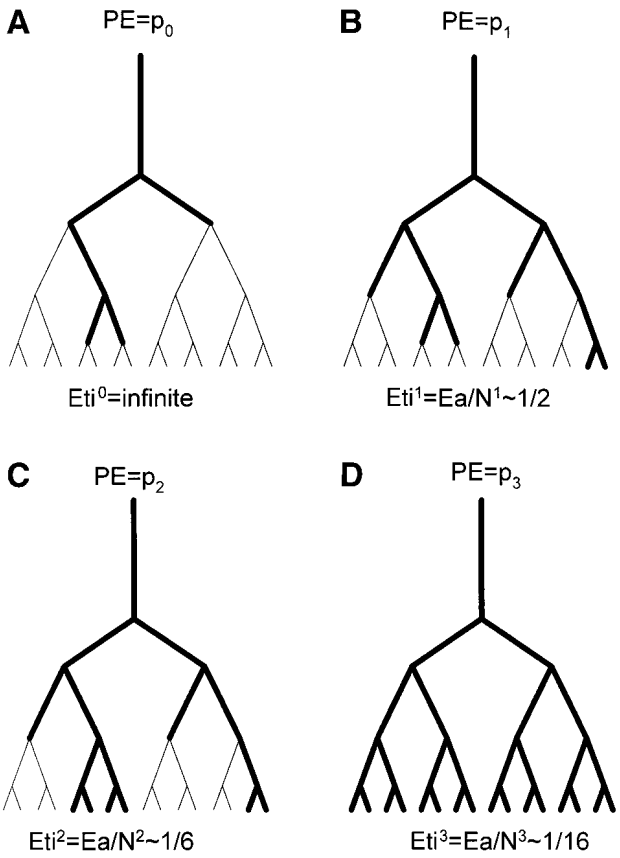

Fig. 3. Schematic representation of airway opening via avalanches in a small 5-generation symmetrical tree. Initially, all airway segments are closed (thin lines) with their respective critical opening threshold pressure. When the external inflation pressure (P_E) reaches the opening threshold pressure of the root $P_E = p_0$ (*A*), 6 airway segments become open (thick lines). The last-generation segments representing the alveoli remain closed. Since Eti is taken proportional to the elastance of a single alveolus (E_A) and is inversely proportional to the number of open alveoli, Eti is infinite in the model. When P_E reaches p_1, additional airways open, including $N^1 = 2$ terminal segments (*B*). Thus the corresponding Eti (Eti^1) will be proportional to $1/N^1 = 1/2$. Further increasing P_E to p_2 opens additional airways (*C*), resulting in a drop in Eti to $Eti^2 \sim 1/6$ and finally filling up the tree when $P_E = p_3$ (*D*) with $Eti^3 \sim 1/16$.

where Eti^1 and Eti^2 are the Eti values and N^1 and N^2 are the number of open terminal units before and immediately after an avalanche, respectively. *Equation 5* shows that since N^1 is smaller than N^2, dE is positive. We can use *Eq. 5* to predict the changes in Eti up to a proportionality factor, E_A, and compare it with experimental values of elastance jumps. The proportionality factor E_A is important, since it is the quantity that reflects the fact that the alveoli are elastic: $E_A = E_A(P_E)$, which is the derivative of the inverse of *Eq. 3* with respect to v. To avoid the problem that we do not know E_A, we normalize the experimental and the numerical jumps with their respective maximum values. Since many jumps are expected to occur with a wide range of dE values, we are interested in the statistical features of the jump sizes. Since the model is stochastic in nature, that is, threshold pressures are randomly distributed over the airway segments, the properties of the model are studied by calculating the probability density distributions of dE and v from 100,000 different realizations of $P_{i,j}$. Additionally, we examined how the distribution function of dE depended on the size of the tree.

RESULTS

Two examples of the input impedance of a subtree separated by 2 s during an inflation are shown in Fig. 4. The real parts are decreasing hyperbolically from a large value of ~8,000 $cmH_2O \cdot l^{-1} \cdot s$ at 1 Hz to a constant of ~1,500 $cmH_2O \cdot l^{-1} \cdot s$ at 40 Hz. The imaginary parts are negative and first decrease, showing a local minimum at ~6 Hz, then increase similarly to the imaginary part of an ideal capacitor. During a slow inflation, one would expect that the magnitude of regional impedance increases with time, since with increasing lung volume, the airways and alveoli become stiffer as a result of stretching their walls. However, our data show that the magnitude of the impedance decreases with increasing time. This can only happen if there was an abrupt opening between the two recordings whereby a larger alveolar region popped open, which resulted in a decrease in impedance magnitude.

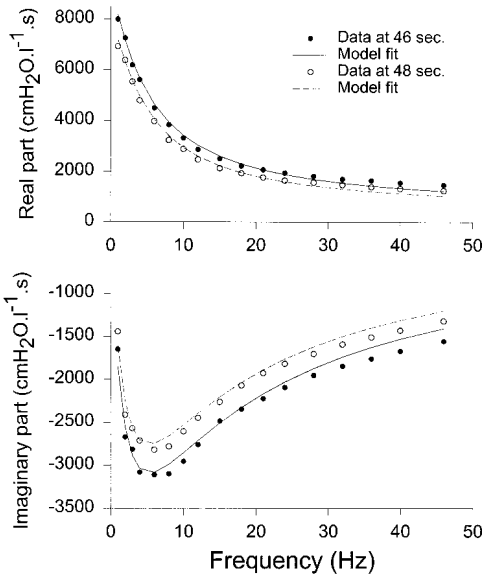

Fig. 4. Real (*top*) and imaginary (*bottom*) parts of regional lung impedances recorded at 46 and 48 s after the start of inflation. The magnitude of impedance decreases between the 2 measurements.

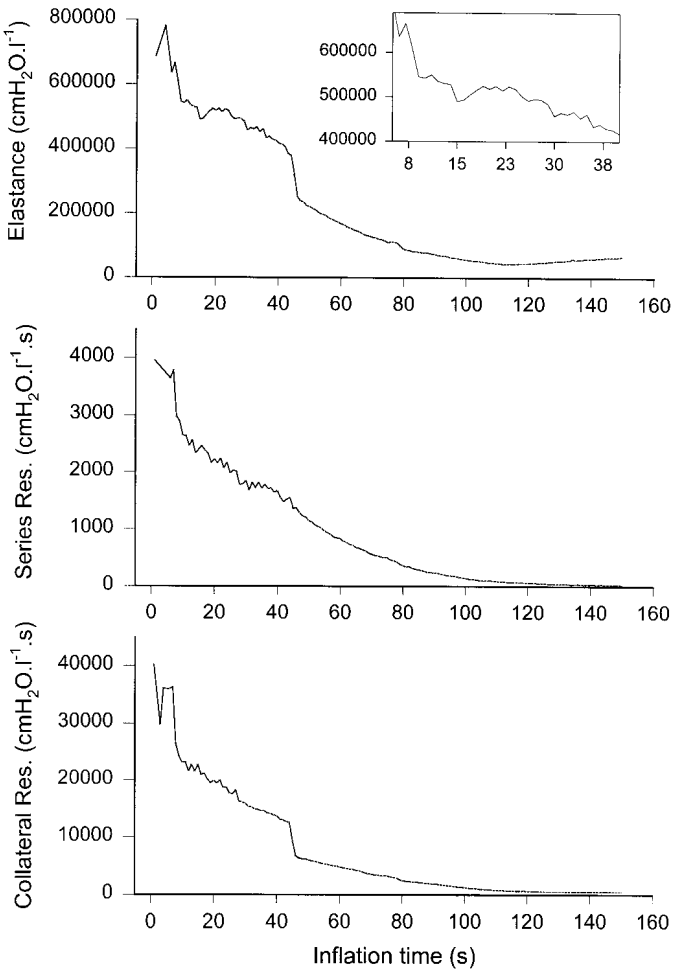

Fig. 5. Eti (*top*), series airway resistance (*middle*), and collateral resistance (*bottom*) as a function of inflation time obtained from model fitting. *Inset*: zoom into the Eti time series.

Figure 4 also shows that the model fits the impedance data reasonably well, although some systematic errors can also be seen. The two Eti values obtained from the fits are 1.3×10^5 and 1.1×10^5 cmH_2O/l, corresponding to the solid and dashed lines, respectively.

The model parameters Eti, R, and R_c are shown as a function of inflation in Fig. 5 for one of the regions. As inflation progresses, all parameters decrease along hyperbolic-like curves. The maximum and minimum values of Eti are 781,200 and 43,980 cmH_2O/l, covering a range of 1.5 orders of magnitude. However, the continuous decrease is interrupted by sudden changes or jump downs. Smaller jumps can also be seen as magnified in the *inset* for Eti. In the middle of inflation, Eti sometimes shows small increases, and, toward the end of inflation, Eti starts continuously increasing. This phenomenon is due to stiffening of the parenchyma. Interestingly, a large jump in R_c occurs simultaneously with Eti at ~45 s, which is not seen in the series resistance R. These patterns changed from region to region and varied between two consecutive inflations even in the same region. Figure 6 demonstrates that our numerical model simulation using a nine-generation tree provides an Eti graph as a function of inflation

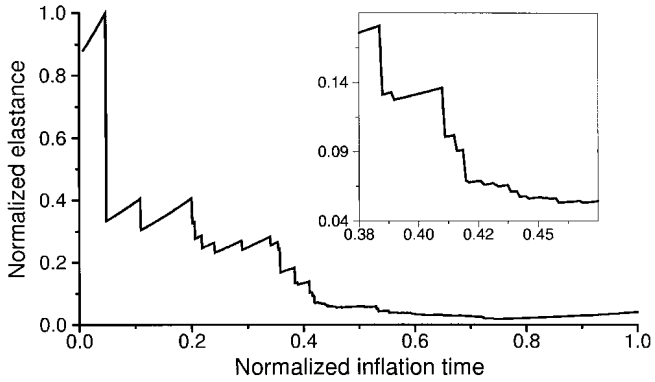

Fig. 6. Normalized Eti as a function of normalized inflation time obtained from simulating airway reopening in a 9-generation symmetrical tree model. *Inset*: zoom into the time series similar to that in Fig. 5, *top*.

time similar to that shown in Fig. 5. Because of the elasticity of the alveolar wall tissue in the model (*Eq. 3*), the simulated Eti as a function of time can even mimic the small increases that follow a jump as well as the gradual increase toward the end of the inflation. Additionally, Fig. 6, *inset*, shows the jumps on a much smaller scale, similar to the experimental data in Fig. 5.

Examining all experimentally obtained Eti graphs (i.e., Eti in Fig. 5*A*), we were able to manually record 1,021 drops in Eti. From the jumps in Eti, dE (defined as in *Eq. 5*), a time series was formed and normalized with the maximum value of dE (Fig. 7*A*). For comparison, a similar time series of dE containing 1,021 elements obtained from the inflation simulations (Fig. 6*A*) is also shown in Fig. 7*B*. In the computer simulation, the numbers of terminal segments before (N^1) and after an avalanche (N^2) were recorded, and the dE was estimated according to *Eq. 5* (where because of elastic walls E_A depends on inflation pressure P_E) and normalized with the largest dE value. Despite the fact that the modeling does not involve any curve fitting or use of measured model parameters, the simulated time series of dE is qualitatively similar to the experimental data both displaying many small jumps with intermittent large jumps. A quantitative comparison can be obtained by examining the statistical features such as the probability density distribution of the time series. The distributions of the experimentally obtained and the simulated dE time series were calculated by binning the dE values using equal size bins in the logarithmic domain. This results in a smoother estimation of the distribution especially for high values of dE, which do not occur frequently. There is a good agreement between the experimental (Fig. 8*A*) and the numerical (Fig. 8*B*) distributions of dE using a nine-generation tree. Both distributions show a region of linear decrease on a log-log graph extending over about two decades of dE values. We also show the distribution of

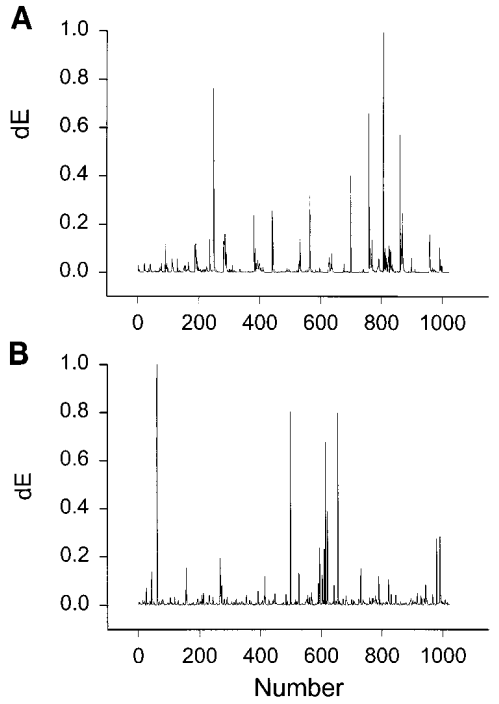

Fig. 7. Time series of drops in Eti (dE) normalized with the maximum value of dE. *A*: dE obtained by manually detecting drops on the Eti vs. time plots (e.g., Fig. 5, *top*). The number of dE values from experiments including data from 11 lobes, 3 regions per lobe, and 2 inflations per lobe, is 1,021. *B*: simulated dE time series including 1,021 points.

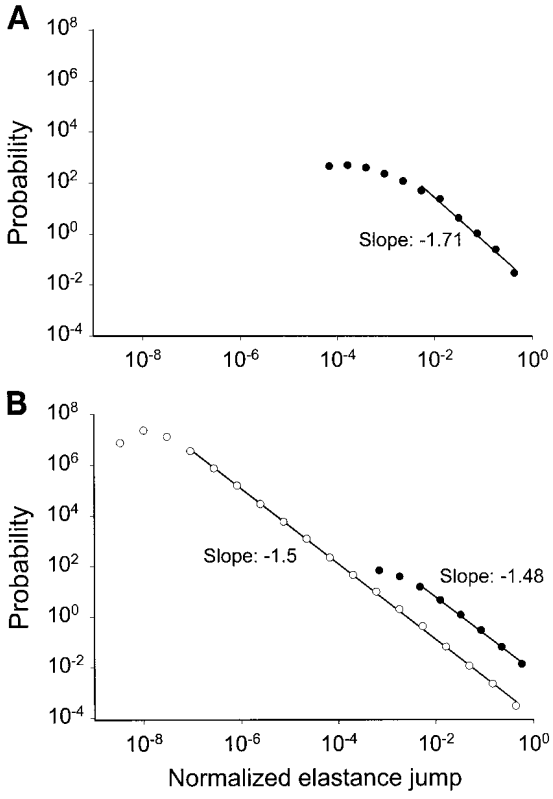

Fig. 8. Log-log plots of the probability density distributions of the relative elastance jumps, dE. *A*: distribution of the dE time series obtained from experimental data in Fig. 7*A*. *B*: distributions of the simulated data. ●, Data in Fig. 7*B*, *bottom*, including the same number of points (1,021) as the experimental data using a 9-generation tree; ○, distribution of simulated data using 100,000 points and a 12-generation tree; solid lines, regions of linear regressions.

dE using a 12-generation tree that exhibits a linear decrease of ~7 decades on the log-log graph. This means that, over the region where the distributions decrease linearly on the log-log graph, the distributions must follow a power law: $p(dE) \sim dE^{-k}$. The negative slope of the linear decrease is the exponent, k, in the power law, which can be estimated by a straight-line fit to the distribution data. The value of k was 1.71 for the measured and 1.5 for the simulated distribution, independently of the size of the tree.

DISCUSSION

The purpose of this work was to experimentally determine the distribution of terminal air spaces that become sequentially open during inflation from the collapsed state of isolated dog lung lobes. For this purpose, we used the technique of Hantos et al. (9) to measure the input impedance of small subtrees of the lobes using 2-mm-OD catheters wedged into the peripheral airways. This measurement system could detect changes in the mechanical parameters of 12–20 generational subtrees according to the airway tree model of Horsfield et al. (12). In particular, this technique allowed us to detect small changes in regional Eti as a function of inflation pressure that could not be detected from pressure-flow measurements at the trachea or from measurement of Ptp.

The primary findings of this study are that airflow resistance and Eti of the subtrees decrease in discrete jumps as a result of discrete openings during inflation. The magnitudes and patterns of these jumps are highly variable, demonstrating that airway reopening observed at the level of these subtrees is a stochastic process reminiscent of the jumps observed in the terminal airway resistances (21, 22, 26). Thus the present data support the notion that airways open in cascades or avalanches (32). Additionally, the distribution of the jumps in Eti is in quantitative agreement with that predicted by a computational model based on the assumption that airways open in avalanches (30).

The most important limitation of the technique is that, to identify Eti, frequencies as low as possible must be included in the input signal. In the original study that introduced this catheter impedance technique, Hantos et al. (9) applied a frequency range of 0.1–48 Hz. The corresponding time resolution was 10 s. Such a poor time resolution would not have allowed us to detect the jumps in Eti seen in Fig. 5. Most of these jumps would have occurred within the time window of the Fourier transform, deteriorating the quality of the impedance spectrum and masking the discrete nature of the openings.

The lowest frequency in our study was chosen to be 1 Hz, which resulted in a 1-s time resolution. The 1 Hz lowest frequency still allowed us to fit a simplified model to the impedance spectra. However, the general quality of the fits did not reach that obtained by Hantos et al. (9), where Z_p was ensemble averaged from several long steady-state recordings including many time windows. The reasons are most likely due to the facts that we had only a single time window for estimating the spectra and we did not include frequencies <1 Hz. The former can lead to less reliable impedance data, whereas the latter can result in reduced reliability of the parameter estimates. As a result, the fluctuations in the parameters in Fig. 5 may, in fact, reflect the presence of numerous discrete opening events occurring within the time window of the Fourier transform (i.e., 1 s). The primary assumption behind the Fourier analysis is stationarity: when an opening occurs within a time window, the corresponding impedance estimate is deteriorated. Although the magnitudes of the series resistance R and the collateral resistance R_c were similar to those found by Hantos et al. (9), the number of jumps that could reliably be identified from the data were not sufficient to carry out a reliable statistical analysis. Additionally, these resistances do not have a clear relationship to the recruited alveolar space, and, hence, we only investigated Eti in this study. In general, for comparable Ptp, the frequency spectra and the values of Eti in this study were similar to those found by Hantos et al. (9). Since during inflation the incremental dynamic elastance of tissue units is expected to rise, the discrete drops in Eti provide evidence that airway opening occurs discontinuously, leading to opening of terminal air spaces of highly varying sizes.

The minimum value of Eti in Fig. 5 is 43,980 cmH_2O/l. This value corresponds to an almost completely open alveolar region inflated to a lung volume close to TLC. This minimum value is much larger than the elastance of the lung; however, it is quite reasonable when we compare it with the lung region supplied by the catheters. The outer diameter of the catheter was 2 mm, and it was fit into an airway at TLC. Thus the airway diameter into which the catheter was fixed must have been ~2 mm. This corresponds to a 17- to 19-generation tree in the airway model of Horsfield et al. (12). The number of terminal segments (alveolar ducts) supplied by such an airway is 331–574. The total number of terminal segments in the airway model of Horsfield et al. is ~150,000. Since we always used the largest lobes from a lung, we estimate the total number of terminal segments in a lobe to be 40,000. If we assume that the catheter supplied 400 segments, the volume of such a region would scale with the ratio 400:40,000 = 0.01. The volume of a dog lobe at TLC is ~300 ml; hence, the volume of the region is estimated to be 300 ml * 0.01 = 3 ml. This is in excellent agreement with the estimates of the supplied volumes we obtained from casts of the peripheral airways as described by Hantos et al. (9). These casts were created by infusing the cast material through catheters similar to those used in the present study. The measured volumes of four casts were 2.8, 3.2, 3.3, and 4.7 ml. Thus the catheter sees ~1% of the total volume of a lobe. The incremental elastance of a dog lung is 10–20 cmH_2O/l at FRC (25), and it would be ≥80 cmH_2O/l at TLC. Thus the lobe elastance close to TLC can be estimated to be ~320 cmH_2O/l depending on the size of the lobe. If the elastance is inversely proportional to regional lung volume, then, on average, the elastance

seen by the catheter would be 320 ÷ 0.01 = 32,000 cmH_2O/l, which is in the range of the minimum Eti of 44,000 cmH_2O/l shown in Fig. 5.

The time series of Eti decreases via smaller and intermittent larger jumps. However, Eti also shows some smaller occasional increases and later a continuous increase toward the end of inflation (Fig. 5). The deterministic increase toward the end of inflation is due to stiffening of the alveolar and airway walls with increasing mean distension. Since in the numerical simulation model we also included alveolar wall elasticity, the Eti predicted by the model will also increase with inflation (Fig. 6). However, we are interested in the rate of decrease in Eti, which was qualitatively similar in the simulations (Fig. 6) and in the measured Eti (Fig. 5). Our simulations in Fig. 6 show that the increases in Eti after a large drop can also be due to stiffening of alveolar tissue. We cannot exclude the possibility, however, that some of the small increases in Eti are due to measurement noise or systematic errors in the fitting of the impedance data. The electrical models (Fig. 2, *C* and *D*) we fit to the impedance data are gross simplifications of the airway structure. During inflation, new collateral channels can open, and the model chosen for that particular inflation may not be the optimal representation of the structure. For example, if first $R_{c,2}$ was open, the tree could be modeled as the network in Fig. 2*D*. However, when $R_{c,1}$ also opens during the same inflation, the tree should be modeled by one of the configurations shown in Fig. 2, *C* and *B*. These model errors (systematic differences between model and data), may occasionally result in an increase in Eti. Unfortunately, these errors are not uniformly distributed. The reason is that the magnitude of impedance decreases more than an order of magnitude from the beginning of inflation to the end, and the absolute error in fitting is a function of the magnitude of the impedance. To see the effects of these fitting errors on our experimental distribution function, we estimated from Fig. 5*A* a maximum value of 0.2×10^5 cmH_2O/l for this deterministic error caused by the fitting procedure. This value corresponds to 0.0027 on the normalized elastance jump scale shown in Fig. 7*A*. Rejecting all values of the normalized elastance jumps <0.0027 from the calculation of the distribution in Fig. 8*A* results in omitting the first three points from the distribution. These first three points, however, were not used in fitting a straight line to the tail of the distribution on the log-log graph. Thus we conclude that possible systematic model errors have no effect on the power law tail of the distribution and, hence, the numerical value of its exponent.

The time series of dE shows many small jumps as well as large jumps (Fig. 7*A*). The simulation results (Fig. 7*B*) are similar to the experimentally derived time series. The probability density distributions of dE estimated from the experimental and simulated data are also similar, showing a linear decrease on the log-log graph over two decades of dE values (Fig. 8). In the numerical simulations, every jump can be detected, including the opening of a single terminal unit. Thus, with the use of the 12-generation tree, the corresponding distribution is much wider, following a power law for very small dE values. The fact that the distributions become flat for small dE ($dE < 10^{-7}$ for a 12-generation tree and $dE < 10^{-2}$ for a 9-generation tree) indicates a finite size effect: the smallest jumps are those that correspond to the opening of a single alveolus. Since the walls of the alveoli are nonlinearly elastic, there is a range of dE values (approximately between 5×10^{-8} and 10^{-7} for the 12-generation tree) corresponding to the opening of a single alveolus where the distribution is more similar to a Gaussian distribution. In contrast, the small jumps are not easily identified from the experimental time series. Toward the end of inflation, adding a small volume (due to opening) to a large volume (already open) will cause Eti to decrease by such a small amount that it can be easily within the experimental noise level. Also, our technique, unfortunately, cannot differentiate among openings occurring independently at different locations but at the same inflation pressure. For example, if two separate openings were triggered within 1 s and in the same time window, we would detect it as a single event with a larger change in Eti. The result is that, instead of two small jumps, we would detect one larger jump. All these effects will reduce the number of small dE values and can lead to a saturation of the dE distribution at much larger values of dE ($\sim 10^{-3}$) than in the computer simulations ($<10^{-7}$).

The experimentally determined exponent is ~13% larger than the numerical one (1.7 vs. 1.5). Several factors could contribute to this discrepancy. First, the tail of the power law distribution is determined by the large values of dE. We point out that one needs many large values of dE to reliably estimate the tail. The number of experimental dE values was only 1,021; hence, the number of large dE values was much less than in the simulations. Second, after insertion of the catheters, the lobes could not be completely degassed. Thus a certain amount of trapped air must have remained in the region supplied by the catheters. To study the effect of trapped air on the distributions of the elastance jumps and the recruited volumes, we repeated some of the simulations using a tree model in which we allowed for trapped air. This was achieved by setting the threshold pressure of a given percentage of the alveoli (or end tips of the tree) to zero and connecting them to the root of the tree. We then inflated the model 10,000 times (see METHODS) and calculated the dE and the recruited volume distribution as a function of the percentage of trapped air. The nature of the distributions was invariant; that is, the elastance jumps and the volume increments followed a power law distribution. However, the exponent k of the elastance distribution was sensitive to the amount of trapped air, increasing from 1.5 with no trapped air to 2 with ~20% trapped air (Fig. 9). The experimental value of $k = 1.71$ corresponds to 1–3% trapped air in the region subtended by the catheter. Because of this dependence of k on trapped air, one should not use *Eq. 5* to transform the experimental dE distribution to estimate the dis-

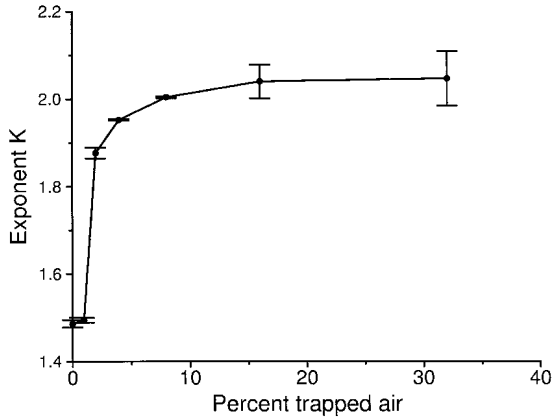

Fig. 9. Exponent of the power law distribution of elastance jumps as a function of trapped air from 10,000 inflations of the 9-generation tree model. Error bars, estimated SD.

tribution of the volume increments. Instead, we can use the full statistics of the simulation (including 100,000 jumps) to estimate the distribution of alveolar volumes that become open during inflation. This distribution is a power law (Fig. 10) with an exponent of 2, in agreement with the predictions of Sujeer et al. (30). Additionally, this distribution was completely independent of the amount of trapped air in the model.

The significance of a power law distribution is that the tail of the distribution is very long compared with, for example, a normal distribution. The tail of a distribution is representative of the relative frequency of occurrence of rare events. Since the tail of a power law can be orders of magnitude larger than the tail of a Gaussian model, the probability of a rare event is also orders of magnitude higher in the power law than in the Gaussian model. Therefore, the process or phenomenon described by a power law distribution does not have a characteristic scale or size that would be largely preferred over other sizes; hence, the power law distribution is said to be "scale free" (29). In our case, a rare event represents a large alveolar region suddenly popping open. If, for example, the alveoli would tend to open in groups of 10–15, then the likelihood of finding a rare event (e.g., a large atelectatic region simultaneously opening) would be small, and the recruited volumes would follow a normal distribution with a mean corresponding to the air volume of ~13 alveoli. The fact, however, that the volume distribution is a power law implies that the probability of having a large alveolar region opening simultaneously is quite high and can be orders of magnitude higher than that for a normal distribution. As a consequence, the measured volumes do not represent the average size of any known physiological unit or structure (e.g., the acinus). Instead, the volume distribution represents a process that can generate a scale-free power law distribution. We argue that the only process that can lead to a power law-recruited volume distribution is airway opening via avalanches. The model developed by Sujeer et al. (30) also predicts that the volume distribution is a power law. The power law volume distribution in that model was obtained by assuming that there is an interaction between reopening of airways and the number of alveoli, because the critical opening pressures are distributed over a tree structure. In particular, airways open in cascades or avalanches, which results in a widely varying number of terminal airways (Fig. 3) and, hence, of recruited alveoli during inflation, the distribution of which follows a power law functional form.

The exponent of a power law distribution fully characterizes the distribution, because the knowledge of the exponent allows us to predict the likelihood of one event compared with another event. The actual numerical value of the exponent has the following significance. First, the smaller the exponent, the slower is the decrease of the tail of the distribution and, hence, the higher the probability of finding rare events. Second, if the process or phenomenon can be mapped onto an existing class of models, a theoretical value for the exponent may be possible. For example, if we associate the normalized reopening pressures with probabilities of airways becoming open, we can map the airway reopening problem onto a sequence of randomly occupying segments in an abstract tree with a given probability p (3), a process called percolation (29). Then increasing the inflation pressure P_E in the lung corresponds to increasing p in percolation. As P_E increases, more and more airways become open, which then corresponds to more clusters of connected segments becoming occupied in the equivalent percolation process. A key quantity in percolation is the distribution of cluster sizes, which is known to follow a power law for certain critical values of p (at the percolation threshold when a large cluster spanning the entire system appears). However, the cluster size distribution is similar to the distribution of recruited volumes. Thus one might expect that known concepts and exponents from percolation theory (29) may be applied to airway reopening. Indeed, the exponent 2 for the volume distri-

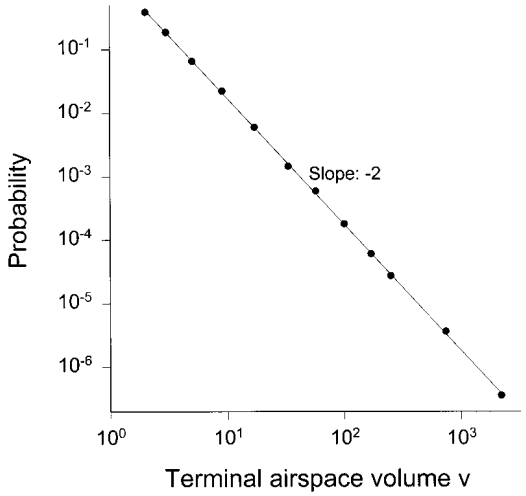

Fig. 10. Log-log plot of the probability density distribution of the terminal air space sizes that become connected to the root of the tree via avalanches. Volume (v) is measured as the number of alveoli opened in an avalanche.

bution can be predicted from percolation (30). Another attractive feature of this mapping is that, for example, in percolation, the cluster size distribution is independent of the details of the system (29). In the model of Sujeer et al. (30), the volume distribution is only marginally affected by airway wall and alveolar wall elasticity or asymmetry in the airway tree: the power law is maintained with the same exponent, but the region over which the power law holds is slightly extended by elasticity and reduced by asymmetry. The primary reason for this robust behavior of the volume distribution is that it has a strong relationship to percolation. Since percolation is a purely geometrical problem, the distribution of recruited volumes is also a geometrical problem and should indeed be invariant of other details of the system. Indeed, power law distributions in the intensity of crackle sound detected during lung inflation similarly arise from the geometric tree structure of the lung (2). In contrast, the distribution of the elastance jumps is not a purely geometrical problem. The reason is that adding a given volume to the open region (adding a constant to N^1 and N^2 in *Eq. 5*) is a nontrivial transformation of the random variable dE in *Eq. 5,* which alters the exponent k of the distribution. Thus we conclude that the power law volume distribution arises from avalanches of airway reopenings triggered by overcoming a hierarchy of critical opening threshold pressures that are distributed widely and relatively independently of generation within the last 10–14 generations of the airway tree in the collapsed lung (32). Our experimental and simulation data in Figs. 5–9 support this interpretation.

Other factors that may influence airway reopening include the nature of the distribution of threshold pressures (30). If, for example, the distribution of threshold pressures is very narrow with a strong generation dependence, such that the threshold pressures do not overlap in consecutive generations, airways do not open in cascade and the size distribution of alveolar volumes is not a power law (30). Additional important factors include the physical properties of the surface film (8, 23) and parenchymal tethering (24, 34). The surface tension, the viscosity, and the non-Newtonian viscoelastic properties (13) of the airway lining fluid certainly have an effect on the dynamics of the local process of opening an airway segment. Parenchymal tethering may also introduce spatial correlations among the reopening of airway segments. However, as long as the distribution of airway opening threshold pressures remains relatively wide and independent of generation, the volume distribution and, hence, the global effect of airway closure on gas exchange are not likely to be influenced much by these factors (30). On the other hand, the opening threshold pressures may change as a result of increased surface tension in certain diseases such as respiratory distress syndrome (1). The effects on reopening of increased film surface tension as in respiratory distress syndrome, increased film viscosity as in cystic fibrosis, or reduced parenchymal tethering as in emphysema were investigated by Perun and Gaver (23, 24). They showed that these factors can prolong the reopening time or increase the critical opening threshold pressures affecting pulmonary function. Sufficiently long reopening times may result in a slow opening process that occurs sequentially, rather than in avalanches. Additionally, if alterations in these physical factors lead to a significant change in the distribution of threshold pressures, the alveolar volume distribution will change, which in turn will also result in significant changes in the pressure-volume curve of the lung, further hindering gas exchange (30).

The implications of knowing the volume distribution are that after a long-term mechanical ventilation "the magnitude and timing of pressure excursions applied at the airway entrance during artificial ventilation may be critical in triggering the avalanche process of alveolar recruitment" (32) and, hence, can have a significant influence on the average number of open airways in a breathing cycle. Indeed, recently, Lefevre et al. (17) found that, in a porcine model of lung injury, introducing "biological variability" in mechanical ventilation by choosing the frequency and tidal volume of ventilation from a normal distribution significantly increases lung compliance and improves gas exchange in the lung. Since airway reopening is a stochastic process (32), variability in tidal volume of mechanical ventilation may help opening of closed airways along the highly nonlinear pressure-volume curve of the atelectatic regions compared with fixed-frequency and -volume ventilation (31). Thus our data support the findings of Lefevre et al. and the predictions of Suki et al. (31), which may therefore have applications in the optimization of ventilation strategies for individuals suffering from lung diseases with significant airway closure and alveolar collapse.

This study was supported by National Science Foundation Grant BES-9813599 and Hungarian Scientific Research Fund Grant OTKA T 016308.

REFERENCES

1. **Adams FHT, Fujiwara T, Emmanouilides G, and Scudder A.** Surface properties and lipids from lungs of infants with hyaline membrane disease. *J Pediatr* 66: 357–364, 1965.
2. **Alencar AM, Hantos Z, Petak F, Tolnai J, Asztalos T, Zapperi S, Andrade JS Jr, Buldyrev SV, Stanley HE, and Suki B.** Scaling behavior in crackle sound during lung inflation. *Phys Rev E* 60: 4659–4663, 1999.
3. **Barabási A-L, Buldyrev S, Stanley HE, and Suki B.** Avalanches in the lung: a statistical mechanical model. *Phys Rev Lett* 76: 2192–2195, 1996.
4. **Crawford ABH, Cotton DJ, Paiva M, and Engel LA.** Effect of airway closure on ventilation distribution. *J Appl Physiol* 66: 2511–2515, 1989.
5. **Csendes T.** Nonlinear parameter estimation by global optimization—efficiency and reliability. *Acta Cybernetica* 8: 361–370, 1988.
6. **Franken H, Clement J, Cauberghs M, and Van de Woestijne KP.** Oscillating flow of a viscous compressible fluid through a rigid tube: a theoretical model. *IEEE Trans Biomed Eng* 28: 416–420, 1981.
7. **Fredberg JJ, Keefe DH, Glass GM, Castile RG, and Frantz ID III.** Alveolar pressure nonhomogeneity during small-amplitude high-frequency oscillation. *J Appl Physiol* 57: 788–800, 1984.

8. **Gaver, DP III, Samsel RW, and Solway J.** Effects of surface tension and viscosity on airway reopening. *J Appl Physiol* 69: 74–85, 1990.
9. **Hantos Z, Peták F, Adamicza A, Asztalos T, Tolnai J, and Fredberg JJ.** Mechanical impedance of the lung periphery. *J Appl Physiol* 83: 1595–1601, 1997.
10. **Hoeppner VH, Cooper DM, Zamel N, Bryan AC, and Levison H.** Relationship between elastic recoil and closing volume in smokers and non-smokers. *Am Rev Respir Dis* 109: 81–86, 1974.
11. **Holley HS, Milic-Emili J, Becklake MR, and Bates DV.** Regional distribution of pulmonary ventilation and perfusion in obesity. *J Clin Invest* 46: 475–481, 1967.
12. **Horsfield K, Kemp W, and Phillips S.** An asymmetrical model of the airways of the dog lung. *J Appl Physiol* 52: 21–26, 1982.
13. **Hsu S-H, Strohl KP, Haxhiu MA, and Jamieson AM.** Role of viscoelasticity in the tube model of airway reopening. II. Non-Newtonian gels and airway simulation. *J Appl Physiol* 80: 1649–1659, 1996.
14. **Hughes JMB, Rosenzweig DY, and Kivitz PB.** Site of airway closure in excised dog lungs: histologic demonstration. *J Appl Physiol* 29: 340–344, 1970.
15. **Jackson AC, Suki B, Ucar M, and Habib RH.** Branching airway network models for analyzing high-frequency lung input impedance. *J Appl Physiol* 75: 217–227, 1993.
16. **Leblanc P, Ruff F, and Milic-Emili J.** Effect of age and body position on "airway closure" in man. *J Appl Physiol* 28: 448–451, 1970.
17. **Lefevre GR, Kowalski SE, Girling LG, Thiessen DB, and Mutch WAC.** Improved arterial oxygenation after oleic acid lung injury in the pig using a computer-controlled mechanical ventilator. *Am J Respir Crit Care Med* 154: 1567–1572, 1996.
18. **Macklem PT, Proctor DF, and Hogg JC.** The stability of peripheral airways. *Respir Physiol* 8: 191–203, 1970.
19. **Milic-Emili J, Henderson JAM, Dolovich MB, Trop D, and Kaneko K.** Regional distribution of inspired air in the lung. *J Appl Physiol* 21: 749–759, 1966.
20. **Naureckas ET, Dawson CA, Gerber BS, Gaver DP III, Gerber HL, Linehan JH, Solway J, and Samsel RW.** Airway reopening pressure in isolated rat lungs. *J Appl Physiol* 76: 1372–1377, 1994.
21. **Otis DR.** *An Investigation of the Mechanisms Responsible for Pulmonary Airway Closure* (Ph.D. thesis). Cambridge, MA: Massachusetts Institute of Technology, 1995.
22. **Otis, DR Jr, Peták F, Hantos Z, Fredberg JJ, and Kamm RD.** Airway closure and reopening assessed by the alveolar capsule oscillation technique. *J Appl Physiol* 80: 2077–2084, 1996.
23. **Perun ML and Gaver DP III.** An experimental model investigation of the opening of a collapsed untethered pulmonary airway. *J Biomech Eng* 117: 245–253, 1995.
24. **Perun ML and Gaver DP III.** Interaction between airway lining fluid forces and parenchymal tethering during pulmonary airway reopening. *J Appl Physiol* 79: 1717–1728, 1995.
25. **Peták F, Hantos Z, Adamicza Á, and Daróczy B.** Partitioning of pulmonary impedance: modeling vs. alveolar capsule approach. *J Appl Physiol* 75: 513–521, 1993.
26. **Peták F, Hantos Z, Adamicza A, Otis DR, and Daróczy B.** Volume dependence of terminal airway impedance in isolated dog lungs (Abstract). *Eur Respir J* 6: 403S, 1993.
27. **Salazar E and Knowles JH.** An analysis of the pressure-volume characteristics of the lung. *J Appl Physiol* 19: 97–104, 1964.
28. **Siegler DIM, Fukuchi Y, and Engel LA.** Influence of bronchomotor tone on ventilation distribution and airway closure in asymptomatic asthma. *Am Rev Respir Dis* 114: 123–130, 1976.
29. **Stauffer D and Aharony A.** *Introduction to Percolation Theory*. London: Taylor & Francis, 1994.
30. **Sujeer MK, Buldyrev SV, Zapperi S, Andrade JS Jr, Stanley HE, and Suki B.** Volume distributions of avalanches in lung inflation: a statistical mechanical approach. *Phys Rev E* 56: 3385–3394, 1997.
31. **Suki B, Alencar AM, Sujeer MK, Lutchen KR, Collins JJ, Andrade JS Jr, Ingenito EP, Zapperi S, and Stanley HE.** Life-support system benefits from noise. *Nature* 393: 127–128, 1998.
32. **Suki B, Barabási A-L, Hantos Z, Peták F, and Stanley HE.** Avalanches and power law behavior in lung inflation. *Nature* 368: 615–618, 1994.
33. **Tepper RS, Gunst SJ, Doerschuk CM, Shen X, and Bray W.** Effect of transpulmonary pressure on airway closure in immature and mature rabbits. *J Appl Physiol* 78: 505–512, 1995.
34. **Yap DYK, Liebkemann WD, Solway J, and Gaver DP III.** Influences of parenchymal tethering on the reopening of closed pulmonary airways. *J Appl Physiol* 76: 2095–2105, 1994.